Nitric oxide generation from heme/copper assembly mediated nitrite reductase activity

By: Shabnam Hematian, Maxime A. Siegler, and Kenneth D. Karlin

Hematian, S., Siegler, M.A. & Karlin, K.D. Nitric oxide generation from heme/copper assembly mediated nitrite reductase activity. *JBIC Journal of Biological Inorganic Chemistry* **19,** 515–528 (2014). https://doi.org/10.1007/s00775-013-1081-6

Abstract:

Nitric oxide (NO) as a cellular signaling molecule and vasodilator regulates a range of physiological and pathological processes. Nitrite (NO_2^-) is recycled in vivo to generate nitric oxide, particularly in physiologic hypoxia and ischemia. The cytochrome *c* oxidase binuclear heme a_3/Cu_B active site is one entity known to be responsible for conversion of cellular nitrite to nitric oxide. We recently reported that a partially reduced heme/copper assembly reduces nitrite ion, producing nitric oxide; the heme serves as the reductant and the cupric ion provides a Lewis acid interaction with nitrite, facilitating nitrite (N–O) bond cleavage (Hematian et al., *J. Am. Chem. Soc.* 134:18912–18915, 2012). To further investigate this nitrite reductase chemistry, copper(II)–nitrito complexes with tridentate and tetradentate ligands were used in this study, where either *O*,*O*′-bidentate or *O*-unidentate modes of nitrite binding to the cupric center are present. To study the role of the reducing ability of the ferrous heme center, two different tetraarylporphyrinate–iron(II) complexes, one with electron-donating *para*-methoxy peripheral substituents and the other with electron-withdrawing 2,6-difluorophenyl substituents, were used. The results show that differing modes of nitrite coordination to the copper(II) ion lead to differing kinetic behavior. Here, also, the ferrous heme is in all cases the source of the reducing equivalent required to convert nitrite to nitric oxide, but the reduction ability of the heme center does not play a key role in the observed overall reaction rate. On the basis of our observations, reaction mechanisms are proposed and discussed in terms of heme/copper heterobinuclear structures.

Keywords: nitric oxide | model compounds | nitrite reductase | nitrite coordination modes | cytochrome c oxidase

Article:

Introduction

The nitrite anion (NO_2^-) is biologically important, for example, in denitrifying bacteria, where it forms from nitrate (NO_3^-) reduction catalyzed by a molybdoenzyme. Then, either copper-containing or heme-containing enzymes reduce the nitrite to nitric oxide (NO), prior to its being reductively coupled to give nitrous oxide (N_2O) and eventually N_2 [1–4]. However, in

mammalian aerobic organisms, until relatively recently, nitrite was considered as a biologically inert one-electron-oxidative end product of endogenous NO metabolism. In fact, this supposedly inert anion can be and is recycled in vivo to generate NO and constitutes a biochemical circulating reservoir for this important signaling molecule, in particular under conditions of physiologic hypoxia and ischemia [5–10].

The classic biological source of NO is nitric oxide synthase (NOS) oxidation of L-arginine [11, 12]. This nitrite reductase chemistry is an important alternative biological source of NO [1–4, 13]. Nitrite reduction to NO involves both pH and oxygen sensor chemistry [13] because of its requirement for one electron and two protons:

$$NO_2^- + 2H^+ + e^- \longrightarrow NO + H_2O$$

Remarkably, the L-arginine–NOS pathway is oxygen-dependent, whereas the nitrite–NO pathway is gradually activated as the oxygen tension falls. Therefore, nitrite-derived NO formation can be considered as a backup system to ensure that there is sufficient NO production in hypoxic conditions where the NO generation (for its signaling functions) in tissues is independent of NOS activity [14].

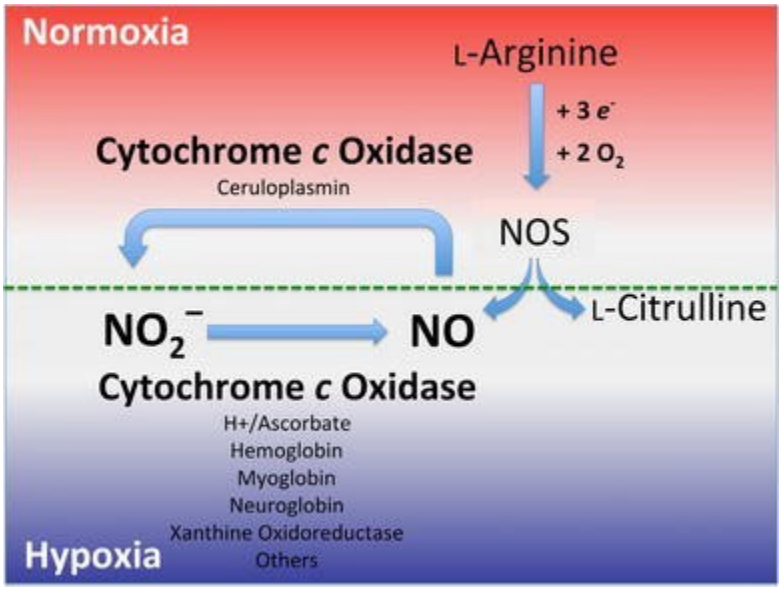

Fig. 1. Nitrite is reduced to nitric oxide by a variety of metal-containing enzymes along the physiological O_2 gradient. Under normal cellular O_2 tensions (normoxia), the critically important signaling molecule nitric oxide is predominantly produced by nitric oxide synthase (NOS). Under hypoxic (low O_2 concentrations) conditions, those associated with cellular stress, the nitrite anion can also serve as an alternative source of nitric oxide generation, via enzymatic reduction processes, including the process associated with cytochrome *c* oxidase

Besides a nonenzymatic conversion of nitrite to NO via acidic disproportionation [5, 15], nitrite as the major intravascular and tissue storage form of NO is readily reduced to NO along a physiological oxygen and pH gradient by a number of proteins/enzymes, such as hemoglobin [16–18], myoglobin [19, 20], neuroglobin [21], xanthine oxidoreductase [8], aldehyde

dehydrogenase [8], cytochrome *c* oxidase (C*c*O; see below), cytochrome *c* [22], and possibly cytochrome P-450 [23–25] (Fig. 1).

Cytochrome *c* oxidase, the terminal enzyme of the mitochondrial respiratory chain and known to catalyze the four-electron reduction of oxygen to water at a heme/copper heterobinuclear centered active site [26–28], has recently been shown to have a novel enzymatic role catalyzing the reduction of nitrite to NO [29, 30]. It is noteworthy that unlike the C*c*O oxidase reaction, which involves four electrons, only one electron is required for the C*c*O nitrite reductase reaction. This nitrite reductase activity is significantly elevated under hypoxic conditions and increases with the lower pH and higher nitrite concentrations that are found in hypoxia [31–34]. These findings are consistent with the following reaction:

$$NO_2^- + C\textit{c}O\text{-}Cu^{II}\text{-}Fe^{II} + H^+ \longrightarrow NO + C\textit{c}O\text{-}Cu^{II}\text{-}Fe^{III} + OH^-$$

However, more recent studies have revealed that the catalytic formation of NO by C*c*O also occurs under normoxia and physiological nitrite concentrations and has been detected in a variety of eukaryotes, including yeast, rat liver, human endothelial cells, bovine heart, calf liver, plants, and algae [29, 31, 35].

In this report, we describe several examples of heme/copper assembly coordination complexes which mediate nitrite reductase chemistry, the one-electron reduction of nitrite to NO. This follows our initial report [36] on this type of chemistry showing a copper(II) complex with coordinated nitrite anion reacts with a ferrous heme, producing NO. Here, we provide additional examples of this newly discovered chemistry, where the exact nature of the heme and/or the copper chelating ligand is modified. For this reaction chemistry, this approach provides (1) differing modes of binding of nitrite to the cupric center, and (2) hemes with differing reducing abilities. For the former, we have examples of nitrite bound to the cupric center with either a tripodal tetradentate pyridyl-alkylamine ligand or a related tridentate alkylamine ligand. For the latter, we compare systems where the heme possesses electron-withdrawing peripheral substituents versus one that is electron-donating. The hope is that via such a systematic approach, we can learn details and fundamental concepts concerning how a heme/copper assembly may affect nitrite reduction chemistry.

Scheme 1 shows the structures of complexes used in this study. The copper complexes are $[(tmpa)Cu^{II}(NO_2)][B(C_6F_5)_4]$ [tmpa is tris(2-pyridylmethylamine)] [36] and the new compound $[(AN)Cu^{II}(NO_2)](CF_3SO_3)$ [AN is 3,3′-iminobis (*N*,*N*-dimethylpropylamine)]; an X-ray crystal structure reveals the binding of nitrite is different from that found for the tmpa-containing complex. The hemes used in this study include the iron(II) complex $(F_8)Fe^{II}$ [F_8 is tetrakis(2,6-difluorophenyl)porphyrinate(2–)] [37, 38] and a heme compound bearing an electron-rich porphyrinate, $(TMPP)Fe^{II}$ [TMPP is tetrakis(4-methoxyphenyl)porphyrinate(2–)]. As shown in Scheme 1, the reactivity observed by using pairwise combinations of the copper–nitrite complex and heme is that reaction of a 1:2 copper/iron complex mixture leads to highly efficient formation of NO, as trapped by the second reduced heme to give a stable ferrous heme–nitrosyl; the initially present copper(II) combines with the ferric heme formed from the redox reaction where nitrite is reduced to NO, and a μ-oxo Fe^{III}–O–Cu^{II} complex is generated as the other product.

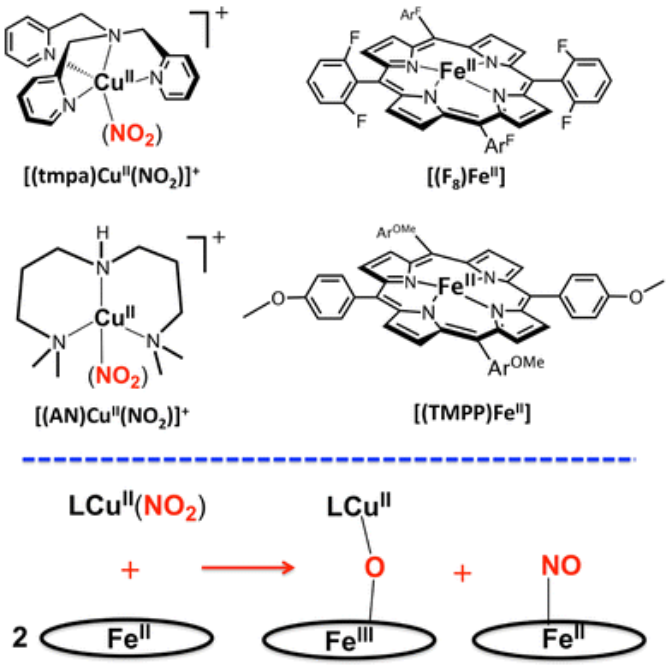

Scheme 1. Nitrite reduction to nitric oxide mediated by heme/copper assemblies: *Top*: Structures of copper and heme complexes used in this study. *Bottom*: Reaction equation representing the reductase chemistry. AN 3,3′-iminobis (*N*,*N*-dimethylpropylamine), F_8 tetrakis(2,6-difluorophenyl)porphyrinate(2–), tmpa tris(2-pyridylmethylamine), TMPP tetrakis(4-methoxyphenyl)porphyrinate(2–)

In fact, the heme/copper C*c*O active site is also responsible for the oxidation of NO to nitrite [36, 39], when NO is in excess and/or O_2 levels increase (recovery from hypoxia). Our research program in large part is concerned with the interplay between reductive or oxidative chemistry at a given heme/copper center, as modulated by metal ion center coordination and redox properties. Thus, as part of these efforts, obtaining an in-depth understanding of the mechanism underlying heme/copper nitrite reductase activity is critical.

Materials and methods

All chemicals and solvents were purchased as commercially available analytical grade unless otherwise stated. Diethyl ether and methanol (MeOH) were used after they had been passed through a 60-cm-long column of activated alumina (Innovative Technologies) under argon. Acetonitrile (MeCN) and pentane were dried by distillation over calcium hydride, and acetone was freshly distilled from Drierite (anhydrous calcium sulfate) under argon prior to use. Tetrahydrofuran (THF) and 2-methyltetrahydrofuran (MeTHF) (Sigma, 673277, inhibitor free) were purified and dried by distillation from sodium/benzophenone ketyl under argon. Dioxygen was dried by passing it through a short column of supported P_4O_{10} (Aquasorb, Mallinkrodt). NO gas was obtained from Matheson Gases and purified following methods previously described in the literature [40–42]. Addition of NO gas to metal complex solutions was effected by transfer via a three-way long syringe needle. Preparation and handling of air-sensitive compounds were performed under an argon atmosphere using standard Schlenk techniques or in an MBraun

Labmaster 130 inert atmosphere (less than 1 ppm O_2, less than 1 ppm H_2O) drybox filled with nitrogen. Deoxygenation of solvents was effected by either repeated freeze/pump/thaw cycles or bubbling with argon for 45–60 min. Electrospray ionization mass spectrometry (ESI-MS) spectra were collected by the Mass Spectrometry Facility at Johns Hopkins University. Elemental analyses were performed by Columbia Analytical Services (Tucson, AZ, USA). Infrared (IR) spectra were obtained using a Thermo Scientific Nicolet Nexus 670 Fourier transform IR (FT-IR) spectrophotometer. UV–vis spectra were recorded with a Cary-50 Bio spectrophotometer equipped with a fiber optic coupler (Varian). The spectrophotometer cells used were made by Quark Glass with a column and pressure/vacuum side stopcock and a 1-cm path length. ^{1}H-NMR spectra were acquired using a Bruker 400-MHz spectrometer. Chemical shifts were reported as δ values relative to an internal standard (tetramethylsilane) and the residual solvent proton peak. Electron paramagnetic resonance (EPR) spectra were recorded with a Bruker EMX spectrometer controlled by a Bruker ER 041 X G microwave bridge operating at X-band (approximately 9.4 GHz).

The compounds $[(tmpa)Cu^{II}(NO_2)][B(C_6F_5)_4]$ [36], $[(tmpa)Cu^{I}(MeCN)][B(C_6F_5)_4]$ [36], $[(AN)Cu^{I}][B(C_6F_5)_4]$ [43], and $(F_8)Fe^{II}$ [37, 38] were synthesized and characterized following methods previously described in the literature. $(TMPP)Fe^{III}(Cl)$ was purchased from TriPorTech (Germany).

$[(AN)Cu^{II}(Cl)](CF_3SO_3)$

Under an argon atmosphere using a Schlenk flask, a solution of AN (375 mg, 2.00 mmol) in 20 mL of freshly distilled MeCN was added to solid $Cu(CF_3SO_3)_2$ (362 mg, 1.00 mmol) and $CuCl_2$ (134 mg, 1.00 mmol). The resulting blue solution was stirred for 30 min at room temperature. The solvent was removed in vacuo, and in the drybox the solid residue was dissolved in a minimal volume of THF. The solution was then filtered, and the filtrate was layered with pentane, affording turquoise blue needles suitable for X-ray crystal structure analysis. After vacuum-drying, the crystals weighed 695 mg (80 % yield). Anal. Calcd for $C_{11}H_{25}ClCuF_3N_3O_3S$: C, 30.34; H, 5.79; N, 9.65. Found: C, 3.54; H, 6.07; N, 9.52. UV–vis spectra [λ_{max}, nm (ε_{max}, M^{-1} cm^{-1})]: 720 (250), 1,025 (227) in acetone (Fig. S1); 722 (227), 1,000 (206) in MeOH (Fig. S2). EPR spectra (X-band spectrometer, ν = 9.428 GHz): $g_2 = 2.116$, $g_3 \approx 2.040$ in acetone at 22 K (Fig. S3); $g_1 = 2.254$, $A_1 = 120$ G, $g_2 = 2.114$, $g_3 = 2.034$ in THF–MeCN (4:1) at 15 K (Fig. S4).

$[(AN)Cu^{II}(NO_2)](CF_3SO_3)$

In the drybox, silver nitrite (77 mg, 0.50 mmol) was added to $[(AN)Cu^{II}(Cl)](CF_3SO_3)$ (218 mg, 0.50 mmol) in 10 mL MeOH, resulting in a green solution. The reaction mixture was then sonicated for 3 h to ensure complete precipitation of AgCl, followed by filtration in the drybox. Slow addition of diethyl ether (30 mL) to the filtrate resulted in crystallization, and the green crystals were dried under a vacuum to afford 205 mg of product (92 %). Anal. Calcd for $C_{11}H_{25}CuF_3N_4O_5S$: C, 29.63; H, 5.65; N, 12.56. Found: C, 30.13; H, 5.98; N, 12.26. UV–vis spectra [λ_{max}, nm (ε_{max}, M^{-1} cm^{-1})]: 702 (327) in acetone (Fig. S1); 702 (309) in MeOH (Fig. S2). EPR spectrum (X-band spectrometer, ν = 9.428 GHz) in acetone at 22 K (Fig. S5): $g_2 = 2.108$, $g_3 \approx 2.051$. FT-IR spectrum (solid) (Fig. S6): $\nu_{as}(NO_2)$ 1,370 cm^{-1}, $\nu_s(NO_2)$

1,110 cm^{-1}, $\delta(NO_2)$ 835 cm^{-1}. Analogous compounds have been previously described: $[(AN)Cu^{II}(NO_2)](NO_3)$ (with the X-ray structure) and $[(AN)Cu^{II}(NO_2)][B(C_6F_5)_4]$ [44].

$(TMPP)Fe^{II}\cdot 1.5H_2O$

Under an argon atmosphere, to a solution of $(TMPP)Fe^{III}(Cl)$ (413 mg, 0.50 mmol) in deoxygenated dichloromethane (150 mL) was added 100 mL of deoxygenated saturated sodium hydrosulfite aqueous solution. The two solutions were vigorously mixed with argon bubbling for about 30 min, during which time the color of the organic layer changed from dark brownish red to bright red. The reaction mixture was allowed to sit for ample time (approximately 20 min) to allow the separation of the two layers. Then the organic layer was allowed to slowly pass through a Schlenk filter tube (coarse porosity) and dried over a small plug of anhydrous sodium sulfate (approximately 6 g). The solvent was removed under a vacuum, yielding 298 mg of product (73 %). Anal. Calcd for $C_{48}H_{39}FeN_4O_{5.5}$: C, 70.68; H, 4.82; N, 6.87. Found: C, 70.88; H, 4.83; N, 6.73. ^{1}H-NMR (pyridine-d_5, 400 MHz; δ, ppm): 8.83 (s, 8H, pyrrole-H), 8.13 (d, 8H, *o*-phenyl-H), 7.29 (d, 8H, *m*-phenyl-H), 4.91 (s, 3H, H_2O), 3.88 (s, 12H, methoxy-H). UV–vis spectra [λ_{max}, nm (ε_{max}, M^{-1} cm^{-1})]: 429 (243,000), 540 (11,400) in acetone (Fig. S7); 430 (256,000), 542 (8,800) in THF (Fig. S8).

$[(TMPP)Fe^{III}–O–Cu^{II}(tmpa)][B(C_6F_5)_4]\cdot 3H_2O\cdot 2MeTHF$

In a 50-mL Schlenk flask equipped with a stir bar, in the drybox, $(TMPP)Fe^{II}\cdot 1.5\ H_2O$ (40 mg, 0.05 mmol) and $[(tmpa)Cu^{I}(MeCN)][B(C_6F_5)_4]$ (53 mg, 0.05 mmol) were dissolved in 10 mL air-free freshly distilled MeTHF. Then dry dioxygen was bubbled through the solution for 2 min and this was accompanied by an immediate color change from dark red to dark green. The mixture was stirred for 20 min at room temperature. The solvent was then removed under a vacuum and solid was further dried under a vacuum for additional 6 h, yielding 86 mg of $[(TMPP)Fe^{III}–O–Cu^{II}(tmpa)][B(C_6F_5)_4]$ (84 %). Anal. Calcd for $C_{100}H_{80}BCuF_{20}FeN_8O_{10}$: C, 58.19; H, 3.91; N, 5.43. Found: C, 58.06; H, 3.86; N, 5.26. UV–vis spectra [λ_{max}, nm (ε_{max}, M^{-1} cm^{-1})]: 443 (252,000), 564 (17,300), 605 (14,700) in acetone (Fig. S8); 441 (189,000), 561 (14,800), 603 (12,100) in MeCN (Fig. S8). ESI-MS spectrum in acetone (Fig. S9): 1,157.3 (TMPP)Fe–O–Cu(tmpa), 788.2 (TMPP)Fe, 1,593.4 $[(TMPP)Fe]_2O$.

In situ generation of $(TMPP)Fe^{II}(NO)$

The ferrous–nitrosyl complex $(TMPP)Fe^{II}(NO)$ was generated in situ by bubbling excess NO gas through the solution of $(TMPP)Fe^{II}$ under a nitrogen atmosphere at room temperature. UV–vis spectra [λ_{max}, nm (ε_{max}, M^{-1} cm^{-1})]: 410 (142,000), 539 (11,900), 614 (4,800) in acetone (Fig. S10); 410 (138,000), 535 (11,500), 610 (4,800) in MeCN (Fig. S11). FT-IR spectrum in acetone: ν(NO) 1,677 cm^{-1} (a published value obtained in dimethylformamide is 1,666 cm^{-1} [45]).

Reaction of 2 equiv of $(F_8)Fe^{II}$ with $[(AN)Cu^{II}(NO_2)](CF_3SO_3)$

In the drybox, to a solution of $(F_8)Fe^{II}\cdot H_2O$ (20.0 mg, 0.024 mmol) in acetone (100 mL) was added $[(AN)Cu^{II}(NO_2)](CF_3SO_3)$ (5.4 mg, 0.012 mmol). After the mixture had been stirred for

3 h, the solvent was removed to yield a brown solid. During the reaction, 305-μL aliquots were withdrawn by syringe every 10 min, diluted with acetone to 5.0 mL, and a UV–vis spectrum was recorded (see "Results"). This procedure allowed quantitative determination of the $[(F_8)Fe^{III}–O–Cu^{II}(AN)]^+$ complex as one of the products and was necessary in order to avoid breakage (by hydrolysis) of the oxo bridge occurring at low concentrations. Formation of a one-to-one mixture of the heme–nitrosyl species $(F_8)Fe^{II}(NO)$ (λ_{max} = 399 nm) and the μ-oxo (λ_{max} = 439 nm) complex was observed. FT-IR spectrum (solid): ν_{NO} = 1,685 cm^{-1}.

Reaction of 2 equiv of $(TMPP)Fe^{II}$ with $[(tmpa)Cu^{II}(NO_2)][B(C_6F_5)_4]$

In a drybox, to a solution of $(TMPP)Fe^{II}\cdot 1.5\ H_2O$ (19.7 mg, 0.024 mmol) in acetone (100 mL) was added $[(tmpa)Cu^{II}(NO_2)][B(C_6F_5)_4]$, (12.9 mg, 0.012 mmol), and after the mixture had been stirred for 3 h, the solvent was removed to yield a brown solid. The preparation of samples for UV–vis analysis during the reaction was done in a manner analogous to the procedure described in "Reaction of 2 equiv of $(F_8)Fe^{II}$ with $[(AN)Cu^{II}(NO_2)](CF_3SO_3)$." UV–vis analysis directly indicated the formation of a one-to-one mixture of the heme–nitrosyl species $(TMPP)Fe^{II}(NO)$ (λ_{max} = 410 nm) and the μ-oxo complex (λ_{max} = 443 nm) (see "Results"). FT-IR spectrum in acetone: ν_{NO} = 1,677 cm^{-1}.

Reaction of 2 equiv of $(TMPP)Fe^{II}$ with $[(AN)Cu^{II}(NO_2)](CF_3SO_3)$

Addition of $[(AN)Cu^{II}(NO_2)](CF_3SO_3)$ (5.4 mg, 0.012 mmol) to a solution of $(TMPP)Fe^{II}\cdot 1.5\ H_2O$ (19.7 mg, 0.024 mmol) in acetone (100 mL) in a drybox was followed by stirring for 3 h. The solvent was then removed to yield a brown solid. The solid product was then dissolved in 10 mL CH_2Cl_2 and was extracted with 25 mL of aqueous NaCl solution (6 mM). The absence of nitrite ion in the aqueous layer was determined by using QUANTOFIX semiquantitative nitrite test strips [36]. The preparation of samples for UV–vis analysis during the reaction was analogous to the procedure described "Reaction of 2 equiv of $(F_8)Fe^{II}$ with $[(AN)Cu^{II}(NO_2)](CF_3SO_3)$." The UV–vis spectrum displays a Soret band at λ_{max} = 419 nm, indicating no μ-oxo complex formation (see "Results"). FT-IR spectrum in acetone: ν_{NO} = 1,677 cm^{-1}.

Reaction of $[(AN)Cu^{I}][B(C_6F_5)_4]$ with nitrite

In the drybox, to a 25 mL acetone solution of $[(AN)Cu^{I}][B(C_6F_5)_4]$ (11.6 mg, 0.012 mmol), $(Bu)_4N(NO_2)$ (3.6 mg, 0.012 mmol) was added, followed by stirring overnight. The UV–vis spectra of the reaction mixture showed no absorbance in the 500–1,100-nm range (Fig. S12), indicating that no redox reaction had occurred.

Reaction of $(TMPP)Fe^{II}$ with nitrite

To a 25 mL acetone solution of $(TMPP)Fe^{II}\cdot 1.5\ H_2O$ (10.2 mg, 0.012 mmol), in the drybox, $(Bu)_4N(NO_2)$ (3.6 mg, 0.012 mmol) was added. The mixture was stirred for several hours, during which time no significant color or UV–vis absorbance changes were observed (Fig. S13), confirming that nitrite reduction does not occur in the absence of Cu(II) as a Lewis acid.

X-ray structure determination

X-ray structure determination of [(AN)Cu^{II}(Cl)](CF_3SO_3) and [(AN)Cu^{II}(NO_2)](CF_3SO_3) was performed at the X-ray diffraction facility at Johns Hopkins University. CIF files have been deposited with the Cambridge Crystallographic Data Centre (CCDC). CCDC 961739 and 961740 contain the supplementary crystallographic data for this article. These data can be obtained free of charge from the CCDC via http://www.ccdc.cam.ac.uk/data_request/cif. All reflection intensities were measured at 110 (2) K using the Agilent Technologies KM4/Xcalibur (detector, Sapphire3) with enhanced graphite-monochromated Mo Kα radiation (λ = 0.71073 Å) with use of the program CrysAlisPro (version 1.171.35.11, Agilent Technologies, 2011). CrysAlisPro (version 1.171.35.11, Agilent Technologies, 2011) was used to refine the cell dimensions. Data reduction was done using CrysAlisPro (version 1.171.35.11, Agilent Technologies, 2011). The structure was solved with the program SHELXS-97 [46] and was refined on F^2 with SHELXL-97 [46]. Analytical numeric absorption corrections based on a multifaceted crystal model were applied using CrysAlisPro (version 1.171.35.11, Agilent Technologies, 2011). The temperature of the data collection was controlled using a Cryojet system (manufactured by Oxford Instruments). The hydrogen atoms (unless otherwise specified) were placed at calculated positions using the instruction AFIX 23 or AFIX 137 with isotropic displacement parameters with values 1.2 or 1.5 times U_{eq} of the attached carbon atoms. For both complexes, the hydrogen atom attached to N2 was found from difference Fourier maps, and the N–H bond distance was restrained using the DFIX instruction.

The structure of [(AN)Cu^{II}(Cl)](CF_3SO_3) is ordered. The absolute configuration was established by anomalous-dispersion effects in diffraction measurements on the crystal, and the Flack parameter refined to −0.017 (9). The structure of [(AN)Cu^{II}(NO_2)](CF_3SO_3) is partly disordered. The trifluoromethanesulfonate counterion is disordered over two orientations [occupancy factor of the major component = 0.586 (4)]. The C4–C3–N1–C1–C2 fragment was also found to be disordered over two orientations [occupancy factor of the major component = 0.759 (4)].

[(AN)Cu^{II}(Cl)](CF_3SO_3)

For [(AN)Cu^{II}(Cl)](CF_3SO_3), the following were found: formula weight 435.39, blue-green lath, 0.49 × 0.21 × 0.12 mm^3, orthorhombic, $P2_12_12_1$ (no. 19), a = 10.3160 (2), b = 10.9961 (2), c = 15.9762 (4) Å, V = 1812.27 (7) $Å^3$, Z = 4, D_x = 1.596 g cm^{-3}, μ = 1.510 mm^{-1}, absorption correction range 0.75–0.863. We measured 9,260 reflections up to a resolution of $(\sin\theta/\lambda)_{max}$ = 0.62 $Å^{-1}$. Of these, 3,665 reflections were unique (R_{int} = 0.0245), of which 3,421 were observed [$I > 2\sigma(I)$]. A total of 215 parameters were refined. R_1/wR_2 [$I > 2\sigma(I)$]: 0.0224/0.0548. R_1/wR_2 (all reflections): 0.0258/0.0561. S = 1.056. Residual electron density was found between −0.24 and 0.34 e^- $Å^{-3}$.

[(AN)Cu^{II}(NO_2)](CF_3SO_3)

For [(AN)Cu^{II}(NO_2)](CF_3SO_3), the following were found: formula weight 445.95, blue-green irregular rod, 0.42 × 0.16 × 0.12 mm^3, monoclinic, $P2_1/n$ (no. 14), a = 10.1675 (2), b = 15.6928 (3), c = 11.7887 (2) Å, β = 90.9584 (16)°, V = 1,880.70 (6) $Å^3$, Z = 4, D_x = 1.575 g cm^{-3}, μ = 1.329 mm^{-1}, absorption correction range 0.706–0.887. We measured

13,996 reflections up to a resolution of $(\sin\theta/\lambda)_{max} = 0.62$ Å^{-1}. Of these, 3,802 reflections were unique ($R_{int} = 0.0396$), of which 3,154 were observed [$I > 2\sigma(I)$]. A total of 342 parameters were refined using 179 restraints. R_1/wR_2 [$I > 2\sigma(I)$]: 0.0354/0.0910. R_1/wR_2 (all reflections): 0.0452/0.0961. $S = 1.053$. Residual electron density was found between −0.42 and 0.53 e^- Å^{-3}.

Results

Copper complex syntheses and X-ray structures

The nitrite complex, $[(AN)Cu^{II}(NO_2)](CF_3SO_3)$, was synthesized by reacting silver nitrite with the chloride precursor $[(AN)Cu^{II}(Cl)](CF_3SO_3)$, and X-ray structures of both compounds were obtained (Fig. 2). The chloride complex of copper(II) is tetracoordinated, with ligation from the three aliphatic nitrogen atoms of the ligand [N(1), N(2), and N(3)], along with the chloride ligand (Cl1). With use of the structural analysis criterion developed by Yang et al. [47], the τ_4 value is 0.69, making the best description of this complex to be of the "seesaw" type. A three-coordinate copper(I) structure with AN has been previously described [43]. The cupric center in $[(AN)Cu^{II}(NO_2)](CF_3SO_3)$ is, however, pentacoordinated by the nitrogen donor atoms of the 3,3′-iminobis(*N*,*N*-dimethylpropylamine) ligand, and O(1) and O(2) of an anisobidentate nitrito ligand. The $Cu–O_{(nitrito)}$ bond distances are unequal, with O1 of the nitrito ligand exhibiting a much weaker interaction with the cupric ion center: the Cu–O1 bond distance is 2.35 Å and the Cu–O2 bond distance is 2.00 Å (see Fig. 2).

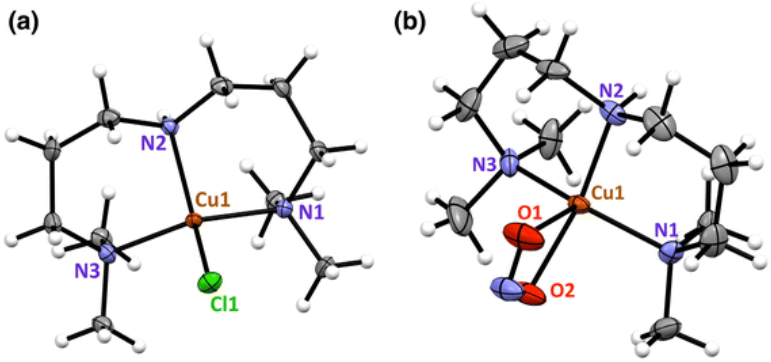

Fig. 2. Displacement ellipsoid plot (50 % probability level) of the copper complexes, showing the atom-labeling scheme. Relevant bond lengths (Å) and angles (°) of $[(AN)Cu^{II}(Cl)]^+$ and $[(AN)Cu^{II}(NO_2)]^+$. **a** $[(AN)Cu^{II}(Cl)]^+$ Cu–N(1), 2.028 (2); Cu–N(2), 1.998 (2); Cu–N(3), 2.031 (2); Cu–Cl(1), 2.227 (6); N(1)–Cu–N(2), 96.5 (7); N(1)–Cu–N(3), 138.6 (4); N(2)–Cu–N(3), 95.7 (7); N(1)–Cu–C1(1), 102.6 (6); N(2)–Cu-Cl(1), 126.6 (8); N(3)–Cu–C1(1), 101.0 (8). **b** $[(AN)Cu^{II}(NO_2)]^+$ Cu–N(1), 2.011 (4); Cu–N(2), 1.993 (2); Cu–N(3), 2.043 (2); Cu–O(1), 2.347 (3); Cu–O(2), 2.002 (2); N(1)–Cu–N(2), 97.6 (1); N(1)–Cu–N(3), 136.8 (1); N(2)–Cu–N(3), 94.8 (9); N(1)–Cu–O(1), 109.0 (1); N(1)–Cu–O(2), 92.9 (1); N(2)–Cu–O(1), 95.7 (9); N(2)–Cu–O(2), 152.0 (6); N(3)–Cu–O(1), 110.6 (7); N(3)–Cu–O(2), 95.0 (1); O(1)–Cu–O(2), 56.2 (8)

By contrast, in our previously structurally characterized complex with the tetradentate tmpa ligand, $[(tmpa)Cu^{II}(NO_2)][B(C_6F_5)_4]$ (Scheme 1), the nitrito ligand is essentially unidentate, with highly different $Cu–O_{(nitrito)}$ bond distances, 1.93 and 2.93 Å [36]. Pentacoordination in this

complex is completed via the four nitrogen donors of tmpa and the single oxygen atom of the nitrito ligand (Structure 1).

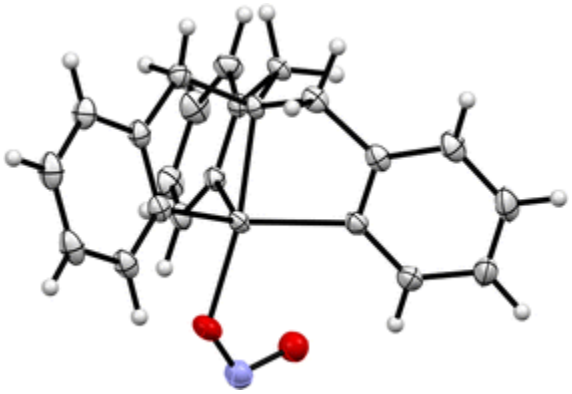

Structure 1. $[(tmpa)Cu^{II}(NO_2)]^+$ [36]

The IR spectrum (Fig. S6) of solid $[(AN)Cu^{II}(NO_2)](CF_3SO_3)$ features nitrite ligand vibrations, further confirming the anisobidentate ONO^- binding ($\Delta\nu = 260\ cm^{-1}$) [48, 49]. Although nitrite vibrations can be assigned with certainty only by isotope labeling, they are tentatively attributed here through the differences in the spectra of the cupric–nitrite complex and its chloride precursor. Consistent with the X-ray structures observed, the EPR spectra of these complexes in frozen solution indicate either tetragonal or rhombically distorted structures, depending on the solvent (Figs. S3, S4, S5).

Nitrite reductase reactivity; cupric–nitrite complexes plus ferrous hemes

In our initial report on this topic [36], we studied the reaction of $[(tmpa)Cu^{II}(NO_2)]^+$ with 2 equiv of the ferrous heme $(F_8)Fe^{II}$, under anaerobic conditions, in acetone at room temperature, and on the basis of spectroscopic analyses, a one-to-one mixture of the heme–nitrosyl species $(F_8)Fe^{II}(NO)$ and the μ-oxo complex $[(F_8)Fe^{III}\text{-}O\text{-}Cu^{II}(tmpa)]^+$ is produced (Scheme 2, top). On the basis of the results of control experiments, the reduced heme provides the one electron required for the reaction, where nitrite (formally NO^+) is reduced and one oxygen atom derived from the nitrite is trapped as an oxo-bridged $Fe^{III}–O–Cu^{II}$ product. See below for further discussion on possible reaction mechanisms.

To expand on the initial study, we decided to compare and contrast the reactivity now using a copper(II)–nitrito complex with a tridentate ligand instead of a tetradentate ligand. We know from many years of study of dioxygen reduction chemistry using copper ion complexes that ligand denticity, along with other factors such as the exact nature of the donor (e.g., alkylamine vs pyridyl) and the chelate ring size (e.g., five-membered vs six-membered ring), governs the structures obtained, the redox properties of derived Cu^{II}/Cu^{I} complexes, and thus the overall reactivity [50–55]. When $[(AN)Cu^{II}(NO_2)]^+$ with a tridentate nitrogen chelate is reacted with 2 equiv of $(F_8)Fe^{II}$, the same overall reaction occurs (Scheme 2). The corresponding μ-oxo complex $[(F_8)Fe^{III}–O–Cu^{II}(AN)]^+$ ($\lambda_{max} = 439$ nm) forms in good yield (more than 80 %), on the basis of the quantitative analyses of UV–vis and EPR spectra (Fig. 3). $[(F_8)Fe^{III}–O–Cu^{II}(AN)]^+$ was previously structurally and spectroscopically characterized [56], but this species is somewhat unstable with respect to hydrolysis owing to its very basic μ-oxo ligand, especially

compared with its analogue [$(F_8)Fe^{III}$–O–Cu^{II}(tmpa)]$^+$) [57, 58]. Thus, some bridge protonation and bridge breaking occurs, leading to the mononuclear complex $(F_8)Fe^{III}$(OH) and (AN)Cu^{II}–X (X is solvent or hydroxide) species. Here, small amounts of these complexes are detected by a combination of UV–vis and EPR spectroscopies. The other product, $(F_8)Fe^{II}$(NO), resulting from capture of NO by one of the two ferrous hemes present in the reaction mixture is obtained in essentially quantitative yield, on the basis of UV–vis spectroscopy (λ_{max} = 399 nm) [36, 59], EPR spectroscopy (Fig. 3), and IR spectroscopy (ν_{NO} = 1,685 cm^{-1}).

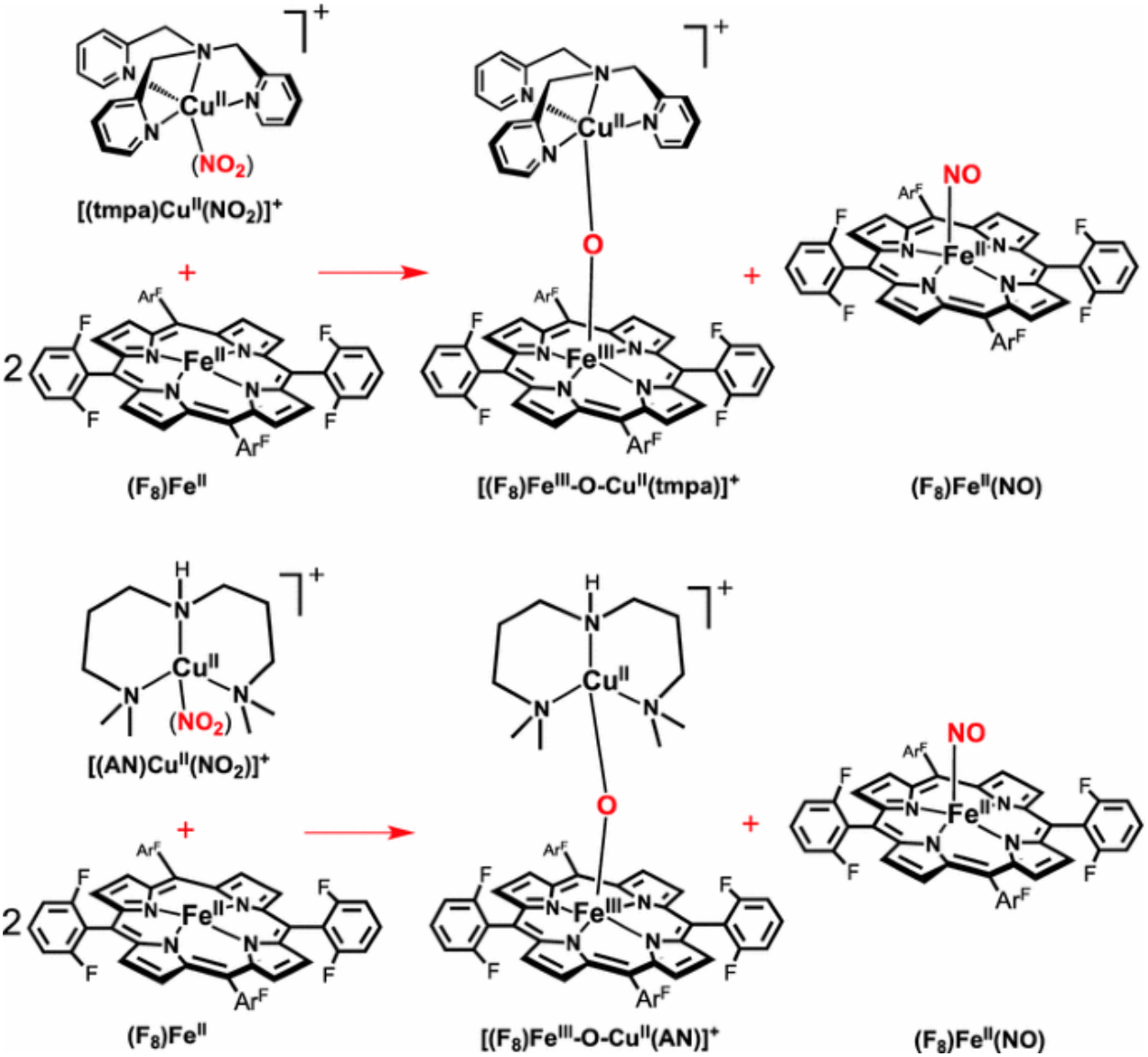

Scheme 2. Reaction of 2 equiv of F_8Fe^{II} with the cupric nitrite complexes: *Top*: with 1 equiv of [(tmpa)Cu^{II}(NO_2)][$B(C_6F_5)_4$]. *Bottom*: with 1 equiv of [(AN)Cu^{II}(NO_2)](CF_3SO_3)

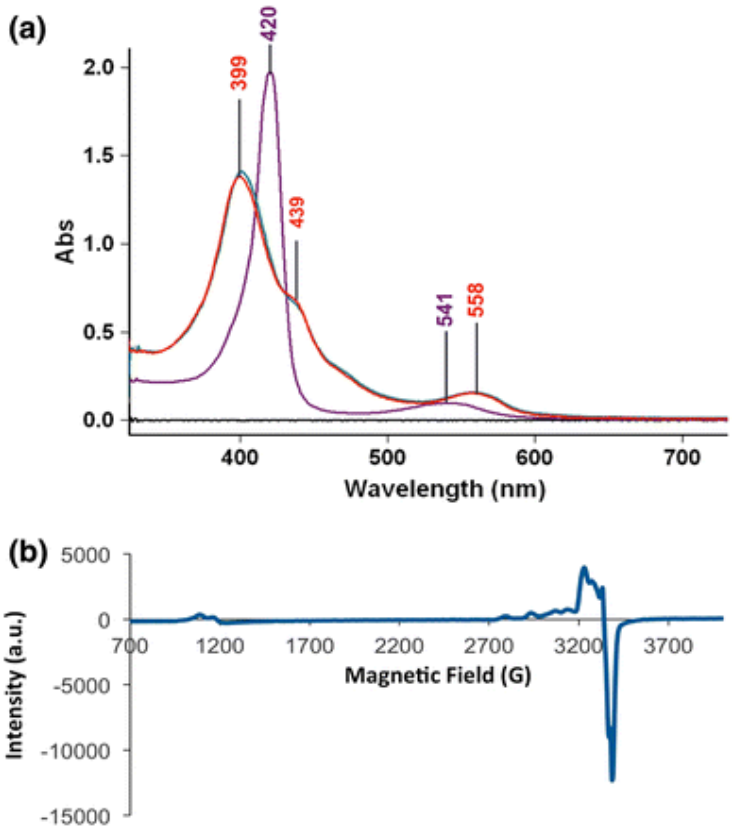

Fig. 3. a UV–vis spectra of $(F_8)Fe^{II}$ (8 μM) [*purple spectrum*; λ_{max} = 420 nm (Soret), 541 nm] and the reaction solution of $(F_8)Fe^{II}$ and $[(AN)Cu^{II}(NO_2)](CF_3SO_3)$ after stirring for 10 min (15 μM) (*green spectrum*) and 1 h (15 μM) [*red spectrum*; λ_{max} = 399 nm (Soret), 439 nm (Soret), and 558 nm] in acetone at room temperature. **b** EPR spectrum of the products of the reaction of $(F_8)Fe^{II}$ and $[(AN)Cu^{II}(NO_2)](CF_3SO_3)$ in acetone at 20 K (2 mM)

When comparing this new system using the nitrite complex $[(AN)Cu^{II}(NO_2)]^+$ with that of the reaction using $[(tmpa)Cu^{II}(NO_2)]^+$, we observe the reaction is roughly twice as fast for the former, on the basis of monitoring the disappearance of the UV–vis band for $(F_8)Fe^{II}$ (λ_{max} = 420 nm). This rate effect may be due to the differing nitrite coordination mode, bidentate versus unidentate in the AN versus the tmpa copper complexes (see "Discussion"). It is worth mentioning that a detailed kinetic analysis was not performed, owing to the exceptional instability of the product $[(F_8)Fe^{III}–O–Cu^{II}(AN)]^+$ when studied at concentrations used for UV–vis monitoring (see "Materials and methods").

In the second set of experiments, to study the role of the reducing ability of the ferrous heme center in nitrite reduction to NO, we used a different heme with strong electron donating peripheral substituents, $(TMPP)Fe^{II}$. This ferrous heme was generated by reduction of $(TMPP)Fe^{III}(Cl)$ under anaerobic conditions and was characterized by UV–vis spectroscopy, ^{1}H-NMR spectroscopy, and elemental analysis. Also, as one of the expected reaction products, the μ-oxo complex $[(TMPP)Fe^{III}–O–Cu^{II}(tmpa)]^+$ (Scheme 3) was synthesized by bubbling dry dioxygen through a one-to-one mixture of the reduced heme and copper mononuclear complexes, and it was characterized by UV–vis spectroscopy, ESI-MS, and elemental analysis. $[(TMPP)Fe^{III}–O–Cu^{II}(tmpa)][B(C_6F_5)_4]$ has a distinctive redshifted Soret band ($\lambda_{max} \approx$ 443 nm;

Fig. S8) [57, 60], which is quite different from other high-spin ferric hemes such as is observed for the μ-oxo porphyrin–iron(III) dimer, $[(TMPP)Fe^{III}]_2O$ [61] ($\lambda_{max} \approx 412$ nm in acetone), and $(TMPP)Fe^{III}(OH)$ ($\lambda_{max} \approx 434$ nm) (Fig. S14). The authentic sample of $[(TMPP)Fe^{II}(NO)$ ($\nu_{NO} = 1{,}677$ cm^{-1}), as the other expected product, was also generated in situ by bubbling excess NO gas into the solution of $[(TMPP)Fe^{II}$ in acetone under a nitrogen atmosphere, and it was characterized by UV–vis and IR spectroscopies.

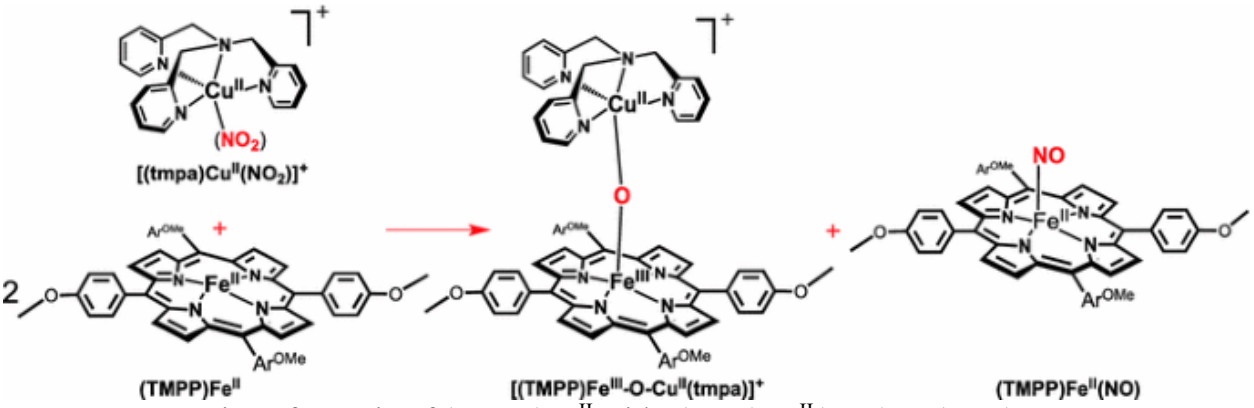

Scheme 3. Reaction of 2 equiv of $(TMPP)Fe^{II}$ with $[(tmpa)Cu^{II}(NO_2)][B(C_6F_5)_4]$

Reacting 1 equiv of the cupric–nitrite complex, $[(tmpa)Cu^{II}(NO_2)]^+$, with 2 equiv of the more electron rich porphyrin, $(TMPP)Fe^{II}$, results in same overall redox reaction, converting nitrite to NO (Scheme 3). We observed the reaction proceeds with about the same rate as for the combination of $(F_8)Fe^{II}$ and $[(tmpa)Cu^{II}(NO_2)]^+$, implying that the greater electron-donating ability of this ferrous heme does not accelerate the nitrite reduction reaction. The quantitative analyses of UV–vis and EPR spectra of the reaction products and authentic samples confirmed the generation of a one-to-one mixture of the ferrous heme–nitrosyl $(TMPP)Fe^{II}(NO)$ ($\lambda_{max} = 410$ nm) and the corresponding μ-oxo complex $[(TMPP)Fe^{III}–O–Cu^{II}(tmpa)]^+$ ($\lambda_{max} = 443$ nm) in high yield (Fig. 4).

In the final system investigated here, we used the copper(II)–nitrite complex with a tridentate (rather than a tetradentate) chelate, with the electron-rich ferrous heme. Reaction of $[(AN)Cu^{II}(NO_2)]^+$ with 2 equiv of $(TMPP)Fe^{II}$ was studied (Scheme 4). IR spectroscopy ($\nu_{NO} = 1{,}677$ cm^{-1}) directly indicated the production of the nitrosyl complex, $(TMPP)Fe^{II}(NO)$. However, according to the UV–vis spectra, there was no formation of the μ-oxo complex $[(TMPP)Fe^{III}–O–Cu^{II}(tmpa)]^+$ (Fig. 5). This may be due to its very basic μ-oxo ligand, resulting in instability toward protonation and hydrolysis. This was further validated when all attempts at the synthesis of the authentic μ-oxo complex by oxidation of reduced complexes (by O_2 bubbling, as described earlier) were unsuccessful, even when using MeTHF as a "dryer" solvent. The species which is instead generated is the μ-hydroxo complex $[(TMPP)Fe^{III}–(OH)–Cu^{II}(tmpa)]^+$ ($\lambda_{max} = 417$ nm), possessing a distinctive Soret band, different from that for the mononuclear complex, $(TMPP)Fe^{III}(OH)$ ($\lambda_{max} = 434$ nm). In spite of the difficulties in this system, comparison of the UV–vis spectra for the actual reaction with those of authentic compounds indicates the nitrite reduction reaction outlined in Scheme 4 occurs in very good yield. Nitrite analysis also confirmed the conversion of nitrite to NO is nearly quantitative, as no trace of nitrite was detected following the reaction.

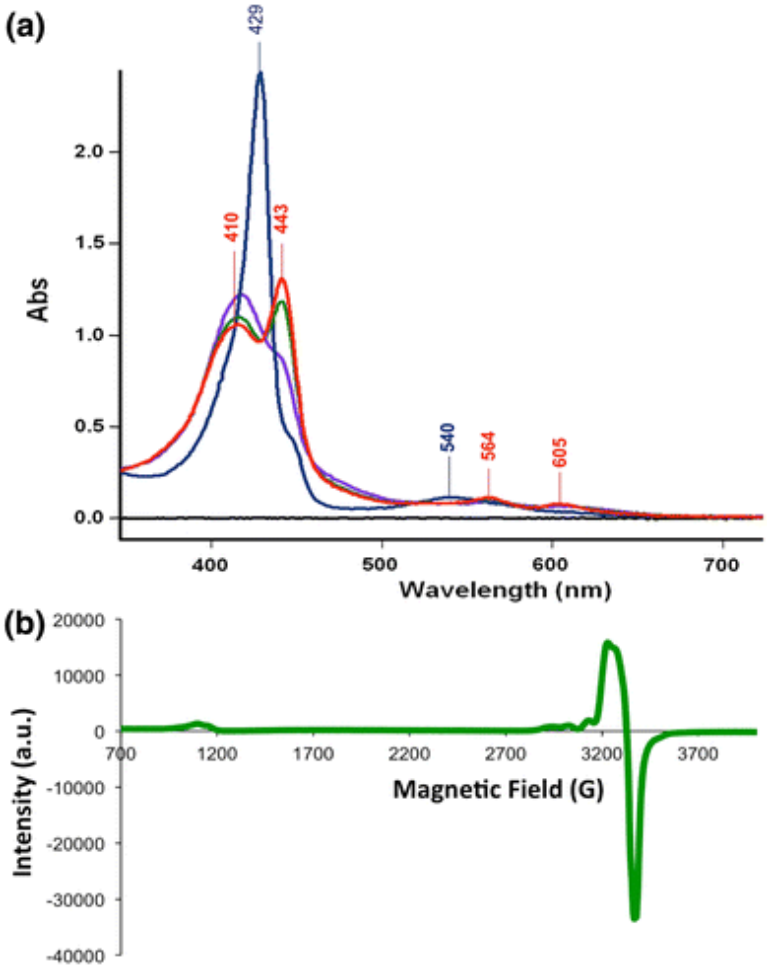

Fig. 4. a UV–vis spectra of (TMPP)Fe^{II} (10 μM) [*blue spectrum*, λ_{max} = 429 nm (Soret), 540 nm] and the reaction solution of (TMPP)Fe^{II} and [(tmpa)$Cu^{II}(NO_2)$][$B(C_6F_5)_4$], after stirring for 10 min (10 μM) (*purple spectrum*) and 1 h (10 μM) [*red spectrum*; λ_{max} = 410 nm (Soret), 443 nm (Soret), 564 nm, and 605 nm) in acetone at room temperature. After the mixture had been stirred for 3 h, the *green spectrum* was recorded. **b** EPR spectrum of the products of the reaction of (TMPP)Fe^{II} and [(tmpa)$Cu^{II}(NO_2)$][$B(C_6F_5)_4$] in acetone at 20 K (2 mM)

The rate of ferrous heme disappearance for this system (Scheme 4) could be semiquantitatively described as being a few times faster than for the reaction of the same heme with the [(tmpa)$Cu^{II}(NO_2)]^+$ analogue (Scheme 3). This observation is the same as that for the reaction of the more electron poor heme, $(F_8)Fe^{II}$, where the reaction of the nitrito complex with the tridentate chelate AN, [(AN)$Cu^{II}(NO_2)]^+$, is again faster than with [(tmpa)$Cu^{II}(NO_2)]^+$ (bearing a tetradentate chelate). Thus, in both cases, faster reduction of nitrite to NO was observed when the ligation of nitrite is bidentate versus unidentate.

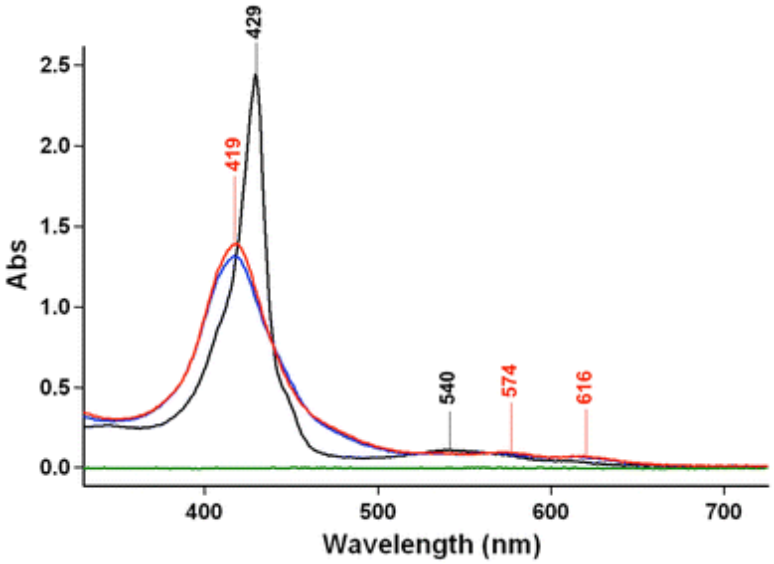

Fig. 5. UV-vis spectra of (TMPP)Fe^{II} (10 μM) [*black spectrum*; λ_{max} = 429 nm (Soret), 540 nm] and the reaction solution of (TMPP)Fe^{II} and [(AN)Cu^{II}(NO_2)](CF_3SO_3), after stirring for 10 min (10 μM) (*blue spectrum*) and 1 h (10 μM) [*red spectrum*; λ_{max} = 410 nm (Soret), 443 nm (Soret), 564 nm, and 605 nm] in acetone at room temperature. See also the text

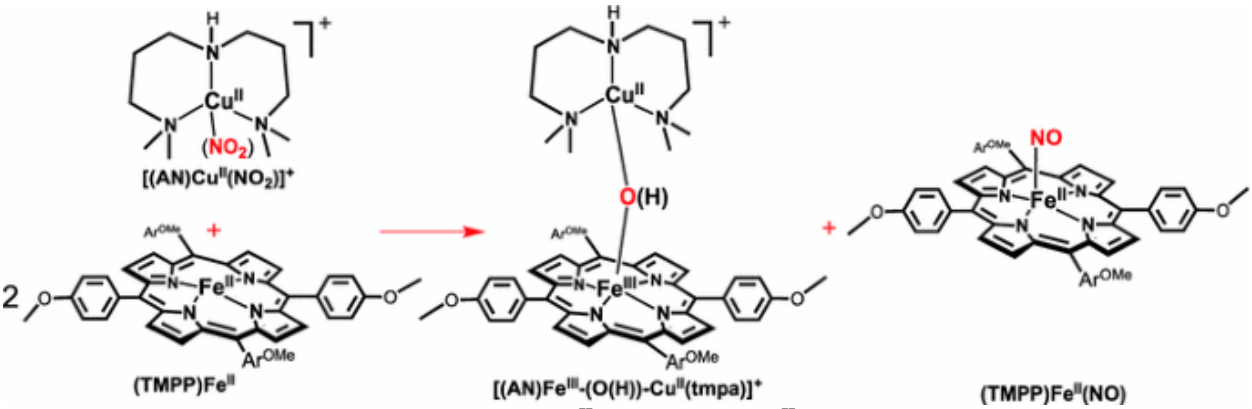

Scheme 4. Reaction of 2 equiv of (TMPP)Fe^{II} with [(AN)Cu^{II}(NO_2)](CF_3SO_3)

Discussion

In "Results," we demonstrated the heme/copper assembly mediated reduction of nitrite to NO, using two different ferrous hemes reacting with either of two cupric–nitrite complexes, one having tetradentate N_4 (tmpa) chelation and the other using a tridentate N_3 (AN) ligand. Very clean and high-yielding reactions occur giving NO, as trapped by our ferrous heme, and an oxo-bridged heme/copper product is also produced. The reaction stoichiometry is indicated in Scheme 1, bottom. Control experiments previously reported for (F_8)Fe^{II} and [(tmpa)Cu^{I}(MeCN)]$^+$ [36] showed that neither of these reduced complexes, nor the combination of the two, is capable of reducing nitrite to NO. [(AN)Cu^{I}]$^+$ and (TMPP)Fe^{II} by themselves are also unreactive to nitrite ion (Figs. S12, S13).[1]

[1] In further control experiments, combinations of reduced complexes, (F_8)Fe^{II}/[(AN)Cu^{I}]$^+$, (TMPP)Fe^{II}/[(tmpa)Cu^{I}(MeCN)]$^+$, and (TMPP)Fe^{II}/[(AN)Cu^{I}]$^+$, were studied. We observed slow reactivity toward

We believe that these reactions to a significant extent relate to what happens in C*c*O nitrite reductase biochemistry. In our synthetic coordination chemistry system, a second heme equivalent is present in order to trap the NO produced, allowing 100 % conversion. If less than two molar equivalents of ferrous heme are added, the reaction occurs only partially, because the NO produced reacts very rapidly with any ferrous heme that has not reacted with the cupric–nitrite complex. In the enzyme, of course this does not occur, but since only oxidized metal ions are present in the active site following nitrite reduction, i.e., iron(III) and copper(II), the NO gas produced escapes since NO binds at best weakly to these oxidized metal ions (Scheme 1, bottom).

As concerns possible reaction mechanisms, we can start by drawing two significant conclusions from the results presented. The first is that the reducing ability of the heme does not seem to matter in determining the course of the overall reaction, and more importantly it does not affect the observed reaction rate (but, of, course in the absence of detailed kinetics). Yet, we can deduce that the electron required for nitrite (formally NO^+) reduction comes from the heme iron(II). We know this because control experiments related to these systems reported earlier [36] showed that a ferric heme with added nitrite does not react with either ligand–copper(I) complex (see Fig. 6).

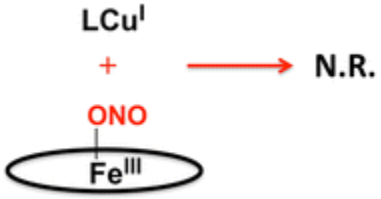

Fig. 6. Reaction of ferric heme nitrite with cuprous complex (*N.R.* is no reaction)

In fact, from electrochemical measurements [36], we know that for the case of ferrous heme $(F_8)Fe^{II}$, the ligand–copper(I) complexes are chemically stronger reductants. So, the ferrous heme supplies the one electron required in the reaction, but when a stronger reductant is used, $(TMPP)Fe^{II}$, as compared with $(F_8)Fe^{II}$, the ferrous heme reduction of nitrite bound to copper(II) does not proceed at an observably greater overall reaction rate. Thus, the electron-transfer reduction apparently does not occur in the rate-determining step.

A second, perhaps key observation is that in a relative sense, the reactions of $[(AN)Cu^{II}(NO_2)]^+$ with ferrous hemes are faster than those of $[(tmpa)Cu^{II}(NO_2)]^+$. We believe that this is an effect of the differing coordination of nitrite in the two cupric complexes. This quite likely leads to differing approaches of the cupric–nitrite complex to form a ferrous heme–(nitrite)–cupric assembly (Scheme 5). As precedent for this supposition, it has been proposed that enzymatic nitrite reduction in heme enzymes occurs either by nitrite nitrogen coordination or by oxygen ligation to the iron and that these lead to alternative courses of reaction with accompanying differing kinetic behavior [62–65].

---

nitrite ion, hours compared with minutes for the Fe^{II}/Cu^{II}–nitrite "parent" reactions, and the final solutions appeared to be a mixtures of the complexes.

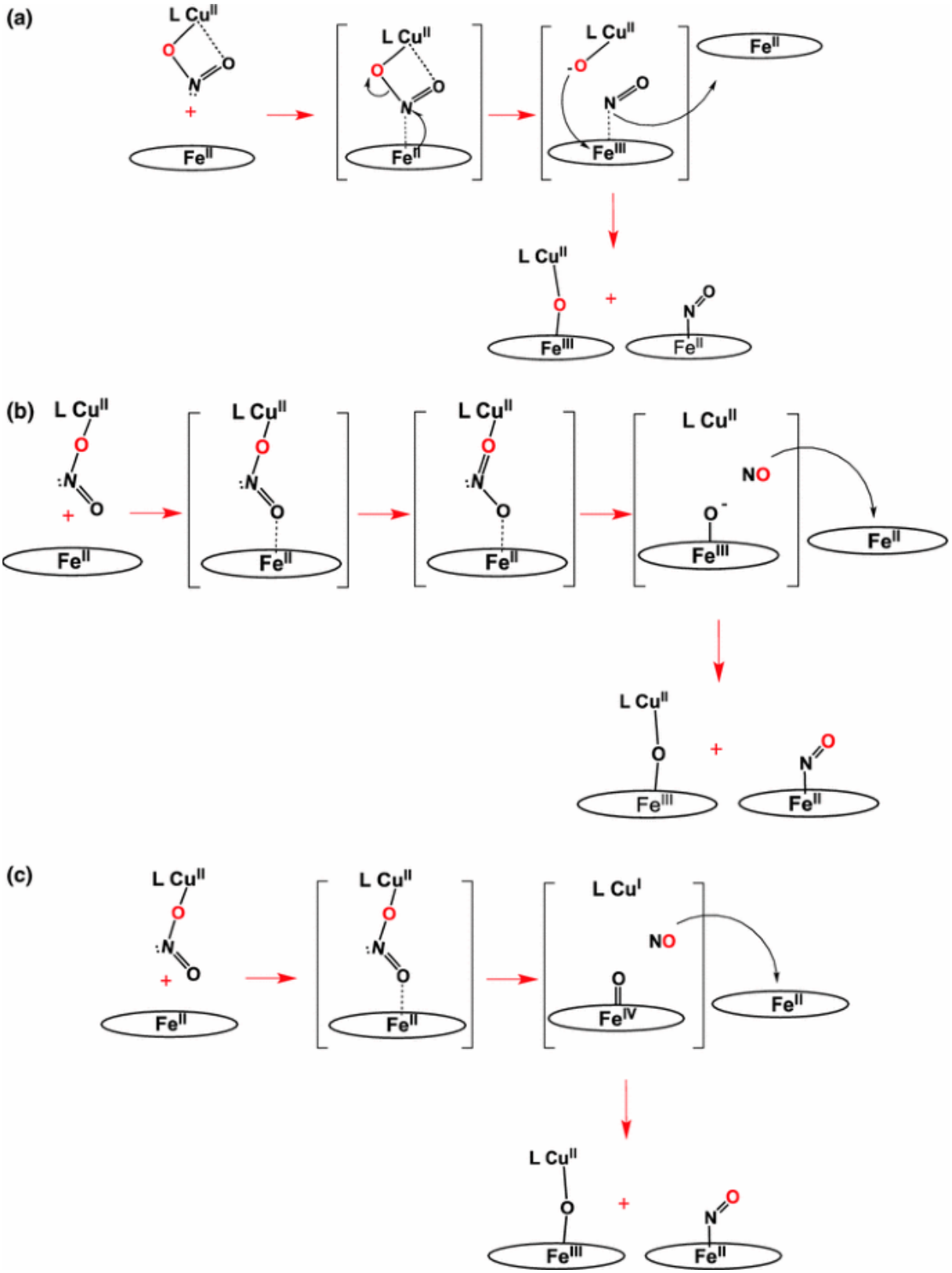

Scheme 5. Proposed reaction mechanisms for nitrite reductase chemistry mediated by the heme/copper assembly. Also, see text

With $[(AN)Cu^{II}(NO_2)]^+$, O,O′ bidentate nitrite coordination (vide supra) allows easier approach of a nitrogen atom to the ferrous heme, i.e., favoring nitrogen (nitro) coordination to the iron(II) ion (Scheme 5a), quite likely in the rate-determining step. Then, electron transfer from iron(II) to the bridged nitrite moiety could readily lead to an $[(AN)Cu^{II}(oxo)]$ (formally oxo is O^{2-}) species and a short-lived ferric–nitrosyl complex; the latter would readily lose NO as a gas, especially in the presence of an exogenous (the second equivalent) ferrous heme, and the ferric ion can easily couple to the cupric–oxo species, giving very kinetically stable μ-oxo compounds $[(porphyrinate)Fe^{III}–O–Cu^{II}(AN)]^+$ (porphyrinate is F_8 or TMPP) (Scheme 5a).

As observed in studies on nitrite reduction by heme protein bacterial nitrite reductases and/or myoglobin [62–65], the approach of the nitrite to the ferrous heme, either via the nitrogen atom or the oxygen atom, is controlled by factors related to the binding pocket, especially nitrite oxygen atom hydrogen bonding from nearby protein amino acid residues. In essence, the cupric ion in the present heme/copper assemblies plays an analogous role, as a Lewis acid surrogate of a proton which (1) orients/directs the nitrite anion to favor iron nitrogen binding [for the $(AN)Cu^{II}$ complex] or oxygen binding [in the case of $(tmpa)Cu^{II}$] and (2) acts as a strong oxo acceptor [note that copper(II) is very oxophilic], which facilitates nitrite (N–O) bond cleavage, leading to subsequent formation of NO along with a μ-oxo heme/copper complex. We cannot, however, rule out a mechanism (not shown) in which the exogenous ferrous heme reduces (by electron transfer) the intermediate ferric–nitrosyl complex (just mentioned) followed by coupling of the Cu^{II}–oxo moiety to the newly produced ferric ion.

For reaction of $[(tmpa)Cu^{II}(NO_2)]^+$ with either ferrous heme, we envision that the oxygen unidentate nitrite copper(II) coordination could very well lead to different reaction mechanisms, as outlined in Scheme 5b and c. Now, the nitrito oxygen atom far from and not coordinated to the cupric center approaches the iron(II) ion, whereupon (1) electron transfer occurs, leading to a short-lived ferric–oxo species, (2) NO forms, escapes, and is trapped by the second ferrous heme, and (3) a cupric complex is generated. The $Fe^{III}–O^-$ couples to the ligand–copper(II) complex, giving $[(porphyrinate)Fe^{III}–O–Cu^{II}(tmpa)]^+$ (Scheme 5b). An alternative but interesting mechanistic proposal would be something like that depicted in Scheme 5c, where the nitrito oxygen atom furthest from copper approaches the iron(II) ion and formally two-electron oxygen-atom transfer occurs, giving a high-valence Fe(IV)=O species, NO gas, and a corresponding cuprous complex; NO gas is again trapped by a second ferrous heme and the Fe(IV)=O and copper(I) moieties couple to give the product $[(porphyrinate)Fe^{III}–O–Cu^{II}(tmpa)]^+$. A precedent for such a mechanism exists. For instance, oxo transfer to an active-site iron has been previously suggested as a mechanistic alternative in nitric oxide reductase biochemistry [66, 67]. Also, we have previously demonstrated that ligand–copper(I) complexes do react with (porphyrinate)Fe(IV)=O species to generate the corresponding μ-oxo heme/copper complex [56].

In addition to the courses of the reaction depicted in Scheme 5b and c, we suggest one other possibility, which is that in all cases, with either $[(tmpa)Cu^{II}(NO_2)]^+$ or $[(AN)Cu^{II}(NO_2)]^+$, nitrite ion nitrogen-atom coordination to the ferrous heme is what leads to a productive reaction, with nitrite (N–O) bond cleavage and NO gas formation. Such coordination is favored on the basis of known (bio)chemistry and expectations from "hard–soft" acid–base considerations. So, even for the chemistry with $[(tmpa)Cu^{II}(NO_2)]^+$, a successful reaction may require dissociation of nitrite from the cupric ion and/or isomerization or rearrangement so the nitrite nitrogen atom can reach

and bind the reduced heme. Perhaps this accounts for the generally slower kinetics observed for the reactions of $[(tmpa)Cu^{II}(NO_2)]^+$ with either ferrous heme complex. Further studies will be required to address these mechanistic considerations.

Conclusion

Our interest in small-molecule activation at heme/copper centers, such as O_2 reduction [68], NO reductive coupling [41, 59], NO oxidation by an oxidized heme/copper center to give nitrite, and nitrite reduction by a partially reduced heme/copper assembly to NO [36], has led us to expand on our previous initial report for the latter, nitrite reductase chemistry with heme/copper assemblies. Such chemistry occurs in the mitochondria of cells, generating additional NO, as needed by cellular demands, such as in hypoxia. Here, with combinations of ferrous or cupric–nitrite complexes, we have shown that NO_2^- can be readily reduced to NO, with the electron coming from the ferrous heme. Clean, stoichiometric, and high-yielding examples of such reactions were presented and were accompanied by detailed chemical and spectroscopic characterization. Although detailed kinetic analyses could not be performed, qualitative but clear trends in reaction rates and results as a function of heme or copper ligation tendencies and/or redox properties were observed. On these bases, possible reaction mechanisms were proposed and discussed, highlighting how the details of particular coordination chemistry situations may influence the course of reactions. Of particular note is that the cupric ion binding mode of nitrite is controlled by the denticity of the chelate on copper, leading to how the coordination of nitrite to the ferrous heme occurs, via either nitrogen-atom or oxygen-atom binding. Such discrimination in enzymes with nitrite reductase activity occurs via heme pocket features, especially hydrogen bonding involving the nitrite anion. In C*c*O, the copper ion may serve exactly such a role, (1) orienting the nitrite for subsequent binding to the reduced heme and (2) acting as an oxo acceptor, as shown by the findings in the present synthetic chemistry study.

Acknowledgments

We are grateful to the US National Institutes of Health for support of this research (GM60353).

Responsible Editors: Lucia Banci and Claudio Luchinat.

References

1. Schopfer MP, Wang J, Karlin KD (2010) Inorg Chem 49:6267–6282
2. Tavares P, Pereira AS, Moura JJG, Moura I (2006) J Inorg Biochem 100:2087–2100
3. Zumft WG (1997) Microbiol Mol Biol Rev 61:533–616
4. Poole RK (2005) Biochem Soc Trans 33:176–180
5. Samouilov A, Kuppusamy P, Zweier JL (1998) Arch Biochem Biophys 357:1–7
6. Dezfulian C, Raat N, Shiva S, Gladwin MT (2007) Cardiovasc Res 75:327–338
7. Lundberg JO, Gladwin MT, Ahluwalia A, Benjamin N, Bryan NS, Butler A, Cabrales P, Fago A, Feelisch M, Ford PC, Freeman BA, Frenneaux M, Friedman J, Kelm M, Kevil CG,

Kim-Shapiro DB, Kozlov AV, Lancaster JR, Lefer DJ, McColl K, McCurry K, Patel RP, Petersson J, Rassaf T, Reutov VP, Richter-Addo GB, Schechter A, Shiva S, Tsuchiya K, van Faassen EE, Webb AJ, Zuckerbraun BS, Zweier JL, Weitzberg E (2009) Nat Chem Biol 5:865–869

8. van Faassen EE, Bahrami S, Feelisch M, Hogg N, Kelm M, Kim-Shapiro DB, Kozlov AV, Li H, Lundberg JO, Mason R, Nohl H, Rassaf T, Samouilov A, Slama-Schwok A, Shiva S, Vanin AF, Weitzberg E, Zweier J, Gladwin MT (2009) Med Res Rev 29:683–741
9. Fukuto JM, Carrington SJ, Tantillo DJ, Harrison JG, Ignarro LJ, Freeman BA, Chen A, Wink DA (2012) Chem Res Toxicol 25:769–793
10. Kozlov AV, Staniek K, Nohl H (1999) FEBS Lett 454:127–130
11. Crane BR (2008) Biochem Soc Trans 036:1149–1154
12. Zhu Y, Silverman RB (2008) Biochemistry 47:2231–2243
13. Gladwin MT, Schechter AN, Kim-Shapiro DB, Patel RP, Hogg N, Shiva S, Cannon RO, Kelm M, Wink DA, Espey MG, Oldfield EH, Pluta RM, Freeman BA, Lancaster JR, Feelisch M, Lundberg JO (2005) Nat Chem Biol 1:308–314
14. Gladwin MT, Shiva S (2009) Circ Res 104:1136–1138
15. Zweier JL, Samouilov A, Kuppusamy P (1999) Biochim Biophys Acta 1411:250–262
16. Cosby K, Partovi KS, Crawford JH, Patel RP, Reiter CD, Martyr S, Yang BK, Waclawiw MA, Zalos G, Xu XL, Huang KT, Shields H, Kim-Shapiro DB, Schechter AN, Cannon RO, Gladwin MT (2003) Nat Med 9:1498–1505
17. Shiva S, Huang Z, Grubina R, Sun JH, Ringwood LA, MacArthur PH, Xu XL, Murphy E, Darley-Usmar VM, Gladwin MT (2007) Circ Res 100:654–661
18. Shiva S, Rassaf T, Patel RP, Gladwin MT (2011) Cardiovasc Res 89:566–573
19. Rassaf T, Flogel U, Drexhage C, Hendgen-Cotta U, Kelm M, Schrader J (2007) Circ Res 100:1749–1754
20. Totzeck M, Hendgen-Cotta UB, Luedike P, Berenbrink M, Klare JP, Steinhoff HJ, Semmler D, Shiva S, Williams D, Kipar A, Gladwin MT, Schrader J, Kelm M, Cossins AR, Rassaf T (2012) Circulation 126:325–334
21. Tiso M, Js Tejero, Basu S, Azarov I, Wang X, Simplaceanu V, Frizzell S, Jayaraman T, Geary L, Shapiro C, Ho C, Shiva S, Kim-Shapiro DB, Gladwin MT (2011) J Biol Chem 286:18277–18289
22. Basu S, Azarova NA, Font MD, King SB, Hogg N, Gladwin MT, Shiva S, Kim-Shapiro DB (2008) J Biol Chem 283:32590–32597
23. Gladwin MT (2005) Nat Chem Biol 1:245–246
24. Lundberg JO, Weitzberg E, Gladwin MT (2008) Nat Rev Drug Discov 7:156–167
25. de Mel A, Murad F, Seifalian AM (2011) Chem Rev 111:5742–5767

26. Babcock GT, Wikström M (1992) Nature 356:301–309

27. Ferguson-Miller S, Babcock GT (1996) Chem Rev 96:2889–2908

28. Kim E, Chufán EE, Kamaraj K, Karlin KD (2004) Chem Rev 104:1077–1133

29. Poyton RO, Ball KA (2011) Discov Med 57:154–159

30. Shiva S (2013) Redox Biol 1:40–44

31. Castello PR, David PS, McClure T, Crook Z, Poyton RO (2006) Cell Metab 3:277–287

32. Gupta KJ, Stoimenova M, Kaiser WM (2005) J Exp Bot 56:2601–2609

33. Castello PR, Woo DK, Ball K, Wojcik J, Liu L, Poyton RO (2008) Proc Natl Acad Sci USA 105:8203–8208

34. Poyton RO, Castello PR, Ball KA, Woo DK, Pan N (2009) Ann N Y Acad Sci 1177:48–56

35. Gupta KJ, Igamberdiev AU (2011) Mitochondrion 11:537–543

36. Hematian S, Siegler MA, Karlin KD (2012) J Am Chem Soc 134:18912–18915

37. Kopf M-A, Neuhold Y-M, Zuberbühler AD, Karlin KD (1999) Inorg Chem 38:3093–3102

38. Ghiladi RA, Kretzer RM, Guzei I, Rheingold AL, Neuhold Y-M, Hatwell KR, Zuberbühler AD, Karlin KD (2001) Inorg Chem 40:5754–5767

39. Torres J, Sharpe MA, Rosquist A, Cooper CE, Wilson MT (2000) FEBS Lett 475:263–266

40. Ford PC, Lorkovic IM (2002) Chem Rev 102:993–1017

41. Wang J, Schopfer MP, Sarjeant AAN, Karlin KD (2009) J Am Chem Soc 131:450–451

42. Schopfer MP, Mondal B, Lee D-H, Sarjeant AAN, Karlin KD (2009) J Am Chem Soc 131:11304–11305

43. Liang H-C, Zhang CX, Henson MJ, Sommer RD, Hatwell KR, Kaderli S, Zuberbuehler AD, Rheingold AL, Solomon EI, Karlin KD (2002) J Am Chem Soc 124:4170–4171

44. Park GY, Deepalatha S, Puiu SC, Lee D-H, Mondal B, Narducci Sarjeant AA, del Rio D, Pau MYM, Solomon EI, Karlin KD (2009) J Biol Inorg Chem 14:1301–1311

45. Vogel KM, Kozlowski PM, Zgierski MZ, Spiro TG (1999) J Am Chem Soc 121:9915–9921

46. Sheldrick GM (2008) Acta Crystallogr Sect A 64:112–122

47. Yang L, Powell DR, Houser RP (2007) Dalton Trans 955–964

48. Mukhopadhyay U, Bernal I, Massoud SS, Mautner FA (2004) Inorg Chim Acta 357:3673–3682

49. Nakamoto K (1997) Infrared and Raman spectra of inorganic and coordination compounds, 5th edn. Wiley Interscience, New York, pp 48–53

50. Quant Hatcher L, Karlin KD (2004) J Biol Inorg Chem 9:669–683

51. Hatcher LQ, Karlin KD (2006) Adv Inorg Chem 58:131–184

52. Chufan EE, Mondal B, Gandhi T, Kim E, Rubie ND, Moenne-Loccoz P, Karlin KD (2007) Inorg Chem 46:6382–6394

53. Kakuda S, Peterson RL, Ohkubo K, Karlin KD, Fukuzumi S (2013) J Am Chem Soc 135:6513–6522

54. Das D, Lee Y-M, Ohkubo K, Nam W, Karlin KD, Fukuzumi S (2013) J Am Chem Soc 135:2825–2834

55. Itoh S (2011) In: Itoh S, Karlin KD (eds) Copper-oxygen chemistry. Wiley, Hoboken, pp 225–282

56. Halime Z, Kieber-Emmons MT, Qayyum MF, Mondal B, Gandhi T, Puiu SC, Chufán EE, Sarjeant AAN, Hodgson KO, Hedman B, Solomon EI, Karlin KD (2010) Inorg Chem 49:3629–3645

57. Fox S, Nanthakumar A, Wikström M, Karlin KD, Blackburn NJ (1996) J Am Chem Soc 118:24–34

58. Obias HV, van Strijdonck GPF, Lee D-H, Ralle M, Blackburn NJ, Karlin KD (1998) J Am Chem Soc 120:9696–9697

59. Wang J, Schopfer MP, Puiu SC, Sarjeant AAN, Karlin KD (2010) Inorg Chem 49:1404–1419

60. Karlin KD, Nanthakumar A, Fox S, Murthy NN, Ravi N, Huynh BH, Orosz RD, Day EP (1994) J Am Chem Soc 116:4753–4763

61. Helms JH, Terhaar LW, Hatfield WE, Harris DL, Jayaraj K, Toney GE, Gold A, Mewborn TD, Pemberton JR (1986) Inorg Chem 25:2334–2337

62. Yi J, Heinecke J, Tan H, Ford PC, Richter-Addo GB (2009) J Am Chem Soc 131:18119–18128

63. Silaghi-Dumitrescu R (2004) Inorg Chem 43:3715–3718

64. Williams PA, Fulop V, Garman EF, Saunders NFW, Ferguson SJ, Hajdu J (1997) Nature 389:406–412

65. Perissinotti LL, Marti MA, Doctorovich F, Luque FJ, Estrin DA (2008) Biochemistry 47:9793–9802

66. Blomberg LM, Blomberg MRA, Siegbahn PEM (2006) Biochim Biophys Acta 1757:240–252

67. Blomberg LM, Blomberg MRA, Siegbahn PEM (2007) J Biol Inorg Chem 12:79–89

68. Halime Z, Kotani H, Li Y, Fukuzumi S, Karlin KD (2011) Proc Natl Acad Sci USA 108:13990–13994